Raman spectrum of NaAlSi2O6jadeite. A quantum mechanical simulation

Raman Spectrum of $NaAlSi_2O_6$ Jadeite. A Quantum Mechanical Simulation.

Mauro Prencipe,[1] Lorenzo Maschio,[2] Bernard Kirtman,[3]
Simone Salustro,[2] Alessandro Erba,[2] and Roberto Dovesi[2]

[1]*Department of Earth Sciences, Università di Torino, Via Valperga Caluso 35, I-10125 Torino, Italy*

[2]*Dipartimento di Chimica, Università di Torino and NIS (Nanostructured Interfaces and Surfaces) Centre of Excellence, Via P. Giuria 7, 10125 Torino, Italy*

[3]*Department of Chemistry and Biochemistry, University of California, Santa Barbara, California 93106, United States*

(Dated: November 29, 2013)

Abstract

The Raman spectrum of $NaAlSi_2O_6$ jadeite is simulated and compared with two recent experimental data sets. In one experiment only 17 (out of 30 symmetry allowed) peaks and a qualitative estimate of the intensities is provided. In the second case the digitalized spectrum is available, from which we have been able to extract 20 evident peaks and an estimate of the relative intensities. The present calculation is based on an ab initio quantum mechanical treatment. Using an *all electron* Gaussian-type basis set, together with the hybrid B3LYP density functional, the full set of 30 active modes and their (polycrystalline and polarized) intensities is obtained. The simulated intensities (not available in a previous study of the same system) permit the two experimental spectra to be reconciled and explain why the missing peaks were not seen. This ultimately leads to excellent agreement between experiment and theory. By artificially varying the mass of the Na^+ and Al^{3+} cations in the simulations, which can be done automatically and at essentially no computational cost, the vibrational modes to which these ions contribute are identified.

We conclude that quantum mechanical simulation can be a very useful complementary tool for the interpretation of experimental Raman spectra.

Keywords: Raman spectrum, frequencies, intensities, quantum mechanical simulation, B3LYP functional, CRYSTAL code

I. INTRODUCTION

In the last decade computer simulation, based on quantum mechanical *ab initio* techniques, has become a powerful and general tool for the investigation of crystalline compounds. Many properties of the ground state (e.g. formation energy, equilibrium geometry, elastic, dielectric, piezoelectric and photoelastic tensors) are simulated nowadays with relatively high accuracy and at low cost.

Recently, it has been shown[1,2] that *ab initio* calculations are extremely useful for interpreting raw infra-red (IR) reflectance spectra of crystalline compounds, particularly in those instances where the presence of many peaks makes it difficult to determine the parameters of the damped oscillators utilized for fitting purposes. It turns out that using the simulated spectrum as an initial guess makes the fitting process much faster and easier.[3,4]

As regards Raman spectra, it has only recently[5–7] become feasible to efficiently compute intensities with the CRYSTAL[8] code. The availability of calculated frequencies and intensities, now permits the full spectrum to be accurately simulated,[9] thereby complementing experiment in cases where the analysis is difficult for one reason or another (such as low crystallinity, presence of impurities, variable orientation, and/or background scattering). In the present paper we will see how simulations allow the Raman spectrum of jadeite ($NaAlSi_2O_6$) to be fully interpreted.

Jadeite (monoclinic, space group $C2/c$) is a chain silicate belonging to the pyroxenes family. Its structure (see Figure 1) consists of chains of corner sharing Si-centred tetrahedra running along the c axis and laterally interconnected by Al and Na-centred polyhedra.[10] According to the structure there are 30 Raman-active modes. However, only a fraction of these has been detected in the available experimental determinations by Gendron *et al.*[11,12] and by Downs.[13] In the paper by Gendron 17 frequencies are reported along with intensities classified qualitatively as weak (w), medium (m), strong (s) or as a shoulder (h). Some of the peaks are also labeled by a (c) to indicate a composite band. The Downs spectrum is in digitized form. In that case we have been able to reliably extract a slightly larger number of peaks, for a total of 20, as well as a quantitative estimate of their intensities. The experimental spectra are reviewed and discussed in detail in Section III.

In the present work the Raman shifts and intensities are calculated by employing the *ab initio* quantum mechanical treatment implemented in the CRYSTAL14[8] code using the hybrid

B3LYP functional,[14,15] which is capable of providing frequency shifts in close agreement with experimental values.[16–25] A preliminary study[26] of this system has previously been carried out. However, since calculated intensities were not available, it was based solely on the peak positions and, in addition the experimental data were limited to the older set obtained by Gendron. In many cases the assignments, based on calculated vibrational frequencies alone, was speculative because (*i*) several modes occur at very close frequency values and, (*ii*) as noted above, many of the allowed peaks were not seen. By using calculated intensities the ambiguities in the assignments are now removed.

This paper is organized as follows. Our computational methods are presented in Section II. Then, in Section III the experimental data are reviewed and analyzed by means of a detailed comparison with our simulations. Finally, a few general conclusions are drawn in Section IV.

II. COMPUTATIONAL METHODS

Calculations were performed using an all-electron Gaussian-type basis set, the hybrid B3LYP functional[14,27] and the CRYSTAL14 code.[8] We utilized an 85-511G contracted basis set on Na[28] as well as 85-11G*, 88-31G* and 8-411G* contractions[29] on Al, Si, and O respectively. The level of accuracy in evaluating the Coulomb and Hartree-Fock exchange series is controlled by five parameters[8], defined by the TOLINTEG keyword in CRYSTAL. These parameters were set to T1=T2=T3=T4=7,T5=16 (see the CRYSTAL manual and Refs. 30,31). The threshold on the total energy for convergence of the self-consistent field (SCF) was set to 10^{-8} Hartree for the orbital optimizations, and to 10^{-10} Hartree for the construction of the Hessian (by numerical differentiation of analytical gradients). Reciprocal space was sampled using a regular sublattice with shrinking factor[8] of 4, corresponding to 24 independent **k** vectors in the irreducible part of the Brillouin zone. The exchange-correlation contribution to the Fock matrix was evaluated by numerical integration over the unit cell volume. Radial and angular points for the integration grid were generated through Gauss-Legendre radial quadrature and Lebedev two-dimensional angular point distributions. In the present work, a pruned grid with 75 radial and 974 angular points was used (see XLGRID keyword in the CRYSTAL manual[8]). Details about the grid generation, the number of points in reciprocal space, and their influence on the accuracy and cost of calculation, can

be found in Refs. 18,19.

The crystal structure was optimized based on analytical energy gradients with respect to fractional atomic coordinates and unit cell parameters,[32–34] within a quasi-Newton scheme utilizing the BFGS algorithm for Hessian updating.[35–38] Default values[8] were chosen for convergence of gradient components as well as nuclear displacements. The calculated equilibrium lattice parameters are reported in Table I. As expected,[24,25] the B3LYP functional overestimates the lattice parameters by 1-2%, and the unit cell volume by about 3% with respect to experiment.

Our calculation of vibrational frequencies at the Γ point was performed within the harmonic approximation. Once the Hessian matrix is calculated, the frequency shifts due to mass substitution can be obtained at essentially zero computational cost by changing the masses in the dynamical matrix since diagonalization is much cheaper than construction of the Hessian. This technique is useful for evaluating the participation of the various atoms in the individual vibrational modes.

The Raman intensity of the Stokes line due to a vibrational mode Q_i with frequency ω_i, that is active due to the gg' component of the polarizability tensor, is given by:

$$I^i_{gg'} \propto C \left(\frac{\partial \alpha_{gg'}}{\partial Q_i} \right)^2 \tag{1}$$

where the prefactor C depends[39] on the laser frequency ω_L:

$$C \sim \frac{1 + n(\omega_i)}{30\omega_i} (\omega_L - \omega_i)^4 \tag{2}$$

and the temperature T through the Bose occupancy factor

$$1 + n(\omega_i) = \left[1 - \exp\Big(- \frac{\hbar\omega_i}{K_B T} \Big) \right]^{-1} \tag{3}$$

Relative intensities were computed using a fully analytical approach[5,6] recently formulated and implemented in CRYSTAL14 program. The formalism is an extension of one developed for infrared intensities.[7,40] It combines analytical gradients[32,33] with solutions of first- and second-order Coupled Perturbed Hartree-Fock/Kohn Sham (CPHF/KS) equations[41,42] for the linear and quadratic orbital response to electric fields in the different Cartesian directions. For the linear response there are three directions to consider; for the quadratic response there are six pairs corresponding to the six independent components of the polarizability tensor. The thresholds for convergence of the Coupled Perturbed equations were set

to the default values.[8] Our procedure is computationally optimal since it avoids numerical differentiation with respect to wave vectors and with respect to atomic coordinates. No perturbation equations for the atomic displacements need to be solved.

III. RESULTS AND DISCUSSION

The primitive unit cell of jadeite contains 20 atoms, giving rise to 60 normal modes, three of which correspond to pure translations. Under the $2/m$ point group of the crystal, the vibrational representation $\Gamma_{\rm tot}$ at the center of the Brillouin zone may be reduced as follows:

$$\Gamma_{\rm tot} = 14A_g + 13A_u + 16B_g + 14B_u$$

The 30 Raman active modes have either A_g or B_g symmetry.

A. Review and Discussion of Experimental Data from Literature

Two different experimental sets of data are reported in Table II, together with our calculated Raman frequencies and intensities (to be discussed in the next sub-section). The first experimental results were reported by Smith and Gendron.[11] Two different spectra, which are virtually identical, were recorded (at λ=514 nm) on archaeological samples. These were complemented a few years later by another spectrum on a sample of geological origin and by four different spectra of a "small bluish-green river pebble ... collected from the bed of the Rio El Tambor".[12] Since all of these spectra are very similar only one of them is shown in Table II, namely the one labeled 44CP07 in Ref. 11.

We were not able to find any other Raman spectra of jadeite in the literature. However, we did retrieve additional measurements from the well-known RRUFF database,[13] where three digitized spectra of jadeite are available, collected at $\lambda = 514$, 532 and 780 nm and T=295 K. We have set up a small program to automatically search for local maxima and determine the relative intensity from the height with respect to the baseline. It is clear that this treatment is crude compared to what may be obtained from commercial curve fitting/deconvolution software since we do not deconvolute overlapping peaks and/or recognize shoulders. On the

other hand, it has the desirable attribute of being simple to apply. Due to our limited experience, of course, we do not yet know whether this treatment will turn out to be generally applicable. We do know that the simulations can easily be done with or without unresolved shoulders for comparison.

Nevertheless, our simple homemade algorithm for determining experimental intensities, together with the calculated frequencies, enabled us to clearly identify 20, 18 and 16 peaks in the three spectra. The spectrum at 514 nm, which provides the largest number of well-defined peaks, was taken to be the best and used for the comparison in Table II (see column labeled Downs[13]). According to the above procedure the list of 20 peaks does not include shoulders, such as the one that appears to the right of peak 13 at 375 cm^{-1} (see Table II and Downs-raw in Figure 2) and was later assigned to mode 14 (calculated at 387 cm^{-1}, see Figure 3).

There is one last comment concerning the three Downs' spectra. Although they are quite similar as regards both frequencies and intensities there is one exception, namely the intensity of the mode assigned as number 24 (calculated at 790 cm^{-1}). This mode is shown in the table with an intensity equal to 11.4% of the peak of maximum intensity, whereas in the other two spectra (not reported) it is 2.5% and 2.9%. The latter values turn out to be much closer (see the next sub-section) to our calculated result (2.8%). This difference in experimental intensities cannot be due to the difference in the laser wavelength adopted for the measurement, which can only have a very small effect.

After measuring the peak heights we attempted to reconstruct the actual Downs spectrum as a superposition of 20 Lorentzian functions. For convenience all the Lorentzians were chosen to have the same width, $\Delta\omega$. Figure 2 shows a comparison between the experimental and reconstructed Downs spectra for three different values of $\Delta\omega$ (6, 8 and 10 cm^{-1}). As can be seen, the $\Delta\omega = 6$ cm^{-1} spectrum shows excellent agreement with experiment in the low frequency region (less than 300 cm^{-1}), whereas $\Delta\omega = 10$ cm^{-1} fits the high frequencies (more than 900 cm^{-1}) better. The intermediate region (300-900 cm^{-1}) is best described by $\Delta\omega = 8$ cm^{-1}. However, all three widths reproduce the experimental spectrum quite well and it is sufficient for our purposes to choose a single uniform width of 8 cm^{-1}, which gives the relative intensities in Table II normalized to a value of 1000 for the most intense peak (mode 23 at calculated frequency of 706 cm^{-1}). The raw and reconstructed Downs spectra with $\Delta\omega = 8$ are shown in Figure 3, where the vertical bars provide the calculated

frequencies and intensities of the 10 modes "missing" from the Downs spectrum.
The experimental spectra of Gendron and Downs match very well with regard to frequencies and more roughly with regard to intensities. For the best match of intensities we adopted the following criteria:

- peaks with a Downs intensity value less than approximately 50 are too weak to have been seen by Gendron (we did not try to establish a Gendron-Downs correspondence for these peaks);
- weak (w in Table II) peaks in the Gendron spectrum correspond to Downs intensity values between approximately 50 and 115;
- medium (m) intensity in the Gendron spectrum corresponds to Downs intensities in the approximate range 115-370;
- intensity values above about 370 in the Downs spectrum are associated with strong (s) peaks in the Gendron spectrum.

With this somewhat arbitrary classification there are just four outliers in the comparison of the two spectra; namely modes 2, 3, 14 and 29. In each case it turns out that the simulated spectrum is much closer to the intensity obtained from Downs' measurements as we will show below.

B. Comparison of Simulation and Experiment

Given the above analysis, we turn now to a comparison of the experimental and simulated spectra. As far as frequencies are concerned, the simulation is in slightly better agreement with the Gendron spectrum (see statistics in Table II), but we do not regard this difference as significant. In either case the extremely good agreement is in line with previous results for silicates.[1] It is, in part, fortuitous since the slight overestimation of the lattice parameters and bond lengths already noted tends to compensate for the overestimation of frequencies that the B3LYP functional usually produces at the experimental geometry, as we have already observed in a number of other instances.[1,2]

The difference in relative intensities is more significant and, as noted in the preceding sub-section, in that case the simulations and the Downs spectrum are in large part consistent with one another. Let us now discuss the four outliers, mentioned at the end of the previous sub-section, where the two experimental spectra disagree. The calculated relative intensity of mode 2 (I=80.3) at 139 cm^{-1} is quite similar to the Downs experimental value (73), which leaves no doubt about this assignment. Mode 3 at 188 cm^{-1} is predicted to be very weak with a relative intensity of 7.7. This is consistent with the fact that it was not seen by Downs, but not with the feature observed by Gendron at $\approx$ 190 cm^{-1}, which was classified as a weak shoulder.

The third outlier is mode 14. It is classified by Gendron as a shoulder to mode 13, but is not resolved by our fitting procedure. We consider it to be an unresolved component of the strong band attribute to mode 13 in the Downs spectrum. Incidentally, modes 12 (predicted to be only 1 cm^{-1} from mode 13) and mode 15 (predicted to be only 2 cm^{-1} from mode 14), are also considered to be components of this same band, which is marked by a square bracket in Table II. Given our assignment of the calculated modes the total intensity is 822 from the simulation and 836 from the Downs experimental spectrum. This set of peaks is discussed further below.

The fourth and last outlier, mode 29, (calculated at 1036 cm^{-1}) is predicted to be strong in the Downs spectrum (I=569), whereas it is proposed as borderline s, m (I in the range 350-390) by Gendron. In this case the simulation intensity value of 467 does not allow us to distinguish between the two experimental data.

We will now focus the remainder of our discussion on the comparison between the simulated and Downs spectra. These spectra are superimposed in Figure 4; the simulated spectrum is computed at the experimental wavelength (514 nm) and temperature (300 K) according to Equations 2 and 3, again with a Lorentzian broadening ω of 8 cm^{-1}.

With the help of Table II and Figure 3 we can understand why 10 out of 30 simulated peaks are not easily identified in the Downs spectrum. Many of the "missing" modes (3, 5, 11, 12, 14, 15, 26 and 28) fall into one or more of the following categories:

- They are within 6 cm^{-1} (the mean absolute difference between experiment and theory in Table II) in predicted frequency of another peak with equal or greater intensity and cannot be resolved (modes 5, 12 and 15). These modes were all discussed above and are included within a square bracket in Table II.

- The nearby peak is a bit further away (up to 12 cm^{-1}) but much more intense so they are still not resolved (modes 14, 26 and 28). Mode 14 has previously been accounted for; mode 28 also appears in the next item.

- The theoretical relative intensity is less than 15. Thus, the peak is probably too weak to have been seen or distinguished from the background (modes 3, 11, 12 and 28). All but mode 11 have been previously considered.

Then there is the more delicate case of mode pairs 16-17 and 18-19 that are not of similar intensity. The members of the pair differ in intensity by factors of 4 and 5.5, respectively, and they are more than 6 cm^{-1} apart. Gendron indicates that mode 17 is a composite. We rely on that interpretation since it is reasonable that mode 17 in Downs is an unresolved composite of 16 and 17. Otherwise, one would expect to see mode 16, which has a simulated intensity of 59 (see further below), in the latter spectrum. As far as the 18-19 pair is concerned, on the one hand Gendron does not use the *mc* designation and, on the other, this pair is not resolved in the Downs spectrum (just like the 16-17 pair). Nonetheless, we believe that the single experimental peak is an unresolved pair. The other possibility is that the B3LYP intensity is a factor of 2 too large. However, that alternative is unlikely since the B3LYP calculations generally underestimate the Downs intensity. A similar underestimate was also noticed by some of the present authors in the case of calcium carbonates.[2] Modes 1 and 30 (with computed intensities of 16.3 and 11.8, respectively) are clearly seen in the Downs spectrum, which means that our criterion (third bullet) for a mode too weak to be seen should be applied judiciously. Actually, mode 1 is close enough to the limit to not be considered an outlier.

Nonetheless, we now see how the calculated intensities enable us to resolve uncertainties in the previous analysis of Prencipe[26] based on Gendron's spectrum alone. Thus, the strong band around 203 cm^{-1} is probably a composite of modes 4 and 5 with the former being the more intense component. Moreover, as we have seen above, the strong band at about 373 cm^{-1}, together with the shoulder at 383 cm^{-1}, arises from the overlap of the two strong A_g modes 13 and 14 as well as the much weaker B_g modes 12 and 15. We see also that the band observed by Gendron at 523 cm^{-1} is the mode 18 + mode 19 pair.

Again, as noted above, the composite mode of medium intensity observed at 988 cm^{-1} is associated with the overlap of modes 26 and 27 and, finally, the strong-medium intensity

band observed at 1036 cm^{-1} corresponds to the calculated strong A_g mode 29, rather than the weak B_g mode 28, as suggested when the calculated intensities were not available.
Mode 24, at a calculated frequency of 790 cm^{-1}, is somewhat puzzling. We have already noted that the two Downs spectra not tabulated agree in intensity with our simulation as does Gendron's characterization of the intensity as being weak. At the moment we cannot explain why the Downs intensity in Table II differs from these results. It is also unclear why Gendron should have observed a weak shoulder at 193 cm^{-1} when mode 3, calculated to be close that frequency, is predicted to have an intensity too small to be seen and, in fact, was not observed by Downs.

C. Directional Raman spectra

The six components of the polarizability tensor provide different Raman profiles of jadeite. The A_g modes give non-vanishing xx, yy, zz and xz components, whereas the B_g modes appear in the xy and yz spectra only.
For a complete definition of the orientation of the lattice with respect to the Cartesian frame, we remind that the three lattice vectors are defined as follows (the standard crystallographic orientation is used): $a = 4.8x + 4.3y$; $b = -4.8x + 4.3y$; $c = -1.6x + 5.0z$.
In Figure 5 we report the six independent single-crystal directional spectra obtained in our calculations, which may be compared with experiment when such data become available. Not only for jadeite but, in general, this would make mode assignments much easier for several reasons:

- Diagonal components will provide signals that are often much larger than off-diagonal ones. For example, in jadeite the xx component of the most intense calculated mode is from 6 to 15 times larger than the highest peak for the yz and xz components, respectively.

  If all directions are lumped together the very intense peaks tend to obscure the weak ones which are, then, not readily identifiable. In the present case the polycrystalline spectrum is dominated by the A_g modes. The B_g modes, which often have much smaller intensity, are unseen in some instances and in others unresolved.

- There can be an unrecognized experimental bias due to preferential orientation in powdered samples.

- Directional spectra are much less "crowded" than polycrystalline spectra and overlapping peaks are rarer, thus reducing the cases of composite and/or unresolved peaks.

D. Isotopic shifts

As a last point, it is worth mentioning the "isotope shift" as a general tool (generated automatically at essentially no additional computational cost in the simulation) that can aid in determining the nature of the vibrational modes. A question is frequently raised concerning the participation of the various ions (here Na^+ and Al^{3+}) in the normal coordinates. In order to answer that question for Na^+, the mass of the ion was arbitrarily increased by 20% and the dynamical matrix was re-diagonalized. In a separate run the same procedure was followed for the Al^{3+} cation. Figure 6 shows the calculated frequency shifts; the horizontal line at -1 cm^{-1} separates shifts that are large from those that are small or negligible. From this figure, we see that the largest shifts occur for B_g modes. Na^+ participates in modes with frequency smaller than 340 cm^{-1}, whereas Al^{3+} contributes to modes with frequencies in the interval 220-620 cm^{-1}. In the overlap interval (220-340 cm^{-1}) both cations can contribute, as is the case for mode 8 at 286 cm^{-1}. Above 620 cm^{-1} the participation of silicon is dominant.

IV. CONCLUSIONS

In this paper the two different experimental Raman spectra available for jadeite have been reconciled and fully analyzed using a new ab initio simulation method at the DFT level with the B3LYP functional and an all-electron Gaussian basis. Peaks that are not revealed experimentally are shown to have low intensity, or to be unresolved. Na and Al "isotope shifts" are employed to identify the modes in which one or both cations participate significantly. Moreover, directional spectra are predicted for the first time. Overall, the present study shows that it is, nowadays, possible to obtain a complete characterization of the Raman spectrum for crystalline compounds with many active modes (30 in the present

case) and that ab initio simulation can be a very useful tool to complement experiment in that regard. The utility of this tool depends upon having the reliably high accuracy that we were able to achieve with the present implementation in the CRYSTAL code.

V. ACKNOWLEDGEMENT

RD and LM acknowledge the CINECA Award N. HP10BLSOR4-2012 for the availability of high performance computing resources and support. Improvements of the CRYSTAL09 code in its MPP version was made possible thanks to the PRACE proposal no. 2011050810 and ISCRA proposal NUCMOTDM - HP10AX8A2M.

Figures

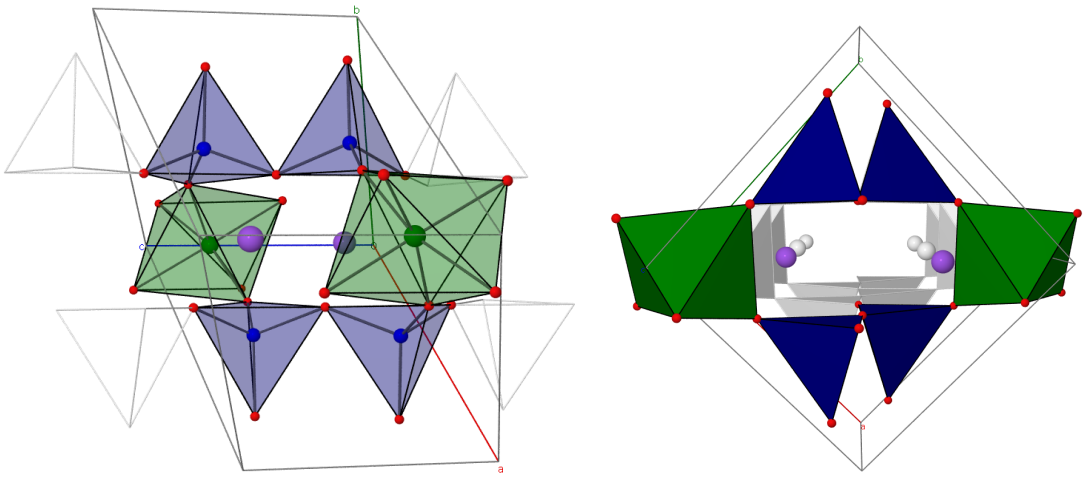

FIG. 1: Structure of jadeite. Within the unit cell SiO_4 polyhedra are in blue, AlO_8 polyhedra are in green, and sodium atoms are in purple. Atoms and polyhedra outside the unit cell are shown in white to display the inosilicate single chain framework.

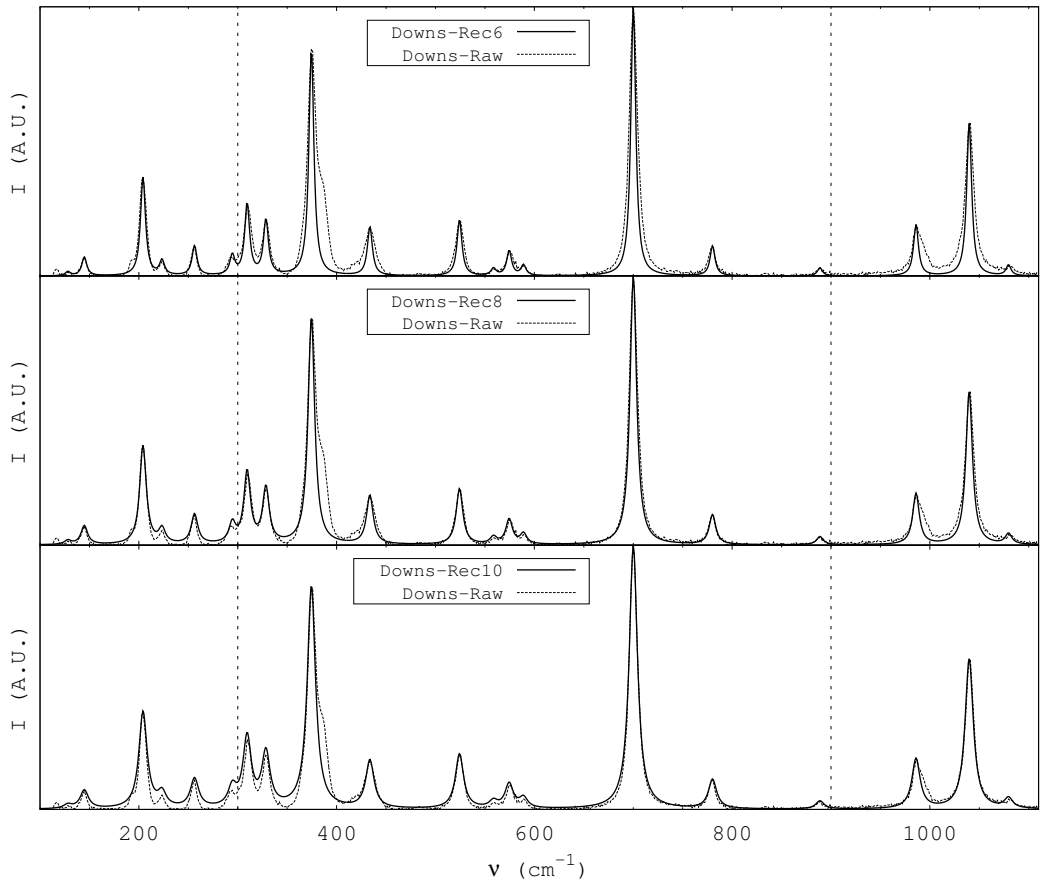

FIG. 2: Comparison between the raw experimental spectrum of Downs (Downs-Raw, dashed line) and the reconstructed (Downs-Rec$\Delta\omega$, continuous line) spectrum obtained by using a linear combination of Lorentzian functions with different widths: $\Delta\omega = 6$ cm^{-1} (top panel); $\Delta\omega = 8$ cm^{-1} (middle panel); $\Delta\omega = 10$ cm^{-1} (bottom panel). The spectrum is divided into three regions by the dashed vertical lines at 300 cm^{-1} and 900 cm^{-1}, as discussed in the text.

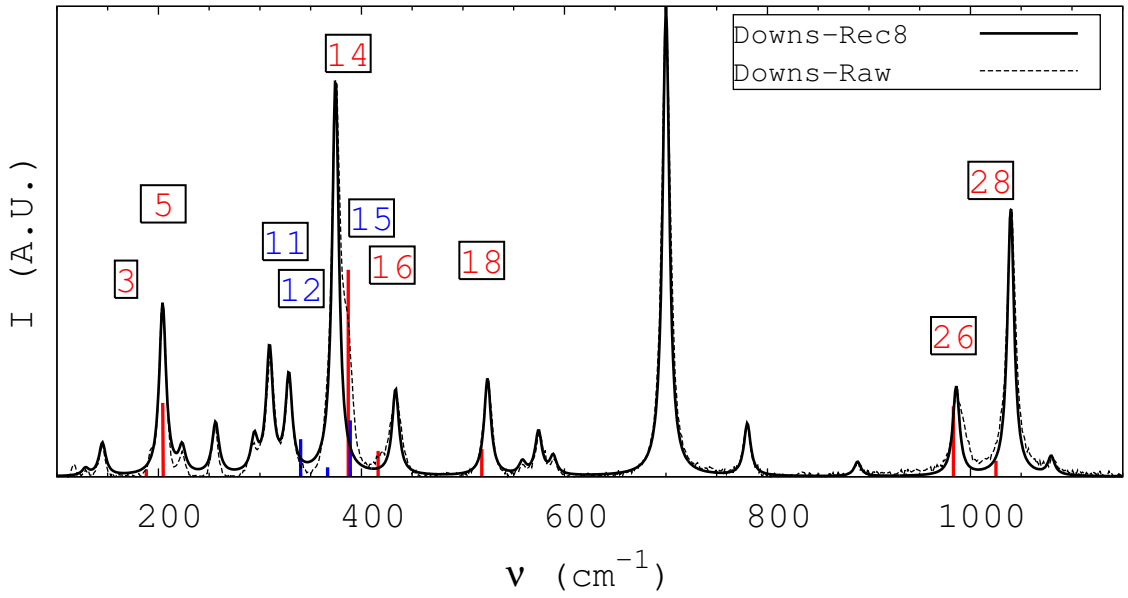

FIG. 3: Experimental Raman spectra of jadeite. Downs-Raw stands for the recorded spectrum as found in Ref.13. Downs-Rec indicates the reconstructed spectrum obtained as a superposition of the 20 Lorentzian curves, whose parameters have been extracted from the Downs-Raw curve by the present authors. Vertical red and blue bars indicate the simulated frequency and intensity of the missing experimental peaks (labels on top are as in Table II). Blue bar intensities have been magnified by a factor 10.

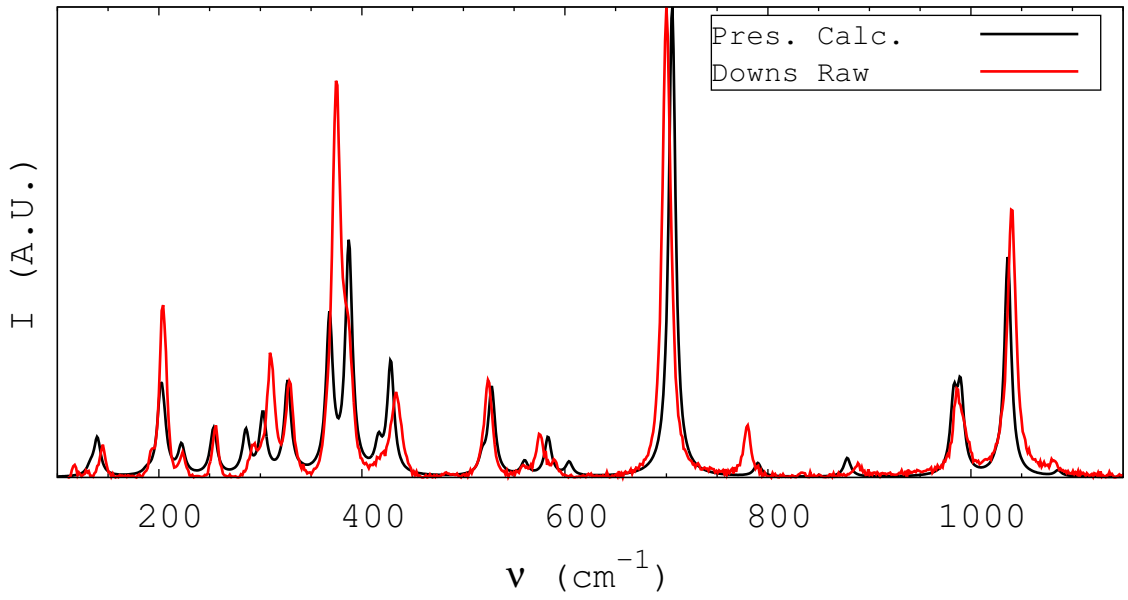

FIG. 4: Experimental[13] Raman spectrum of (polycrystalline) jadeite as compared to the simulated spectrum calculated at 514 nm wavelength and 300 K.

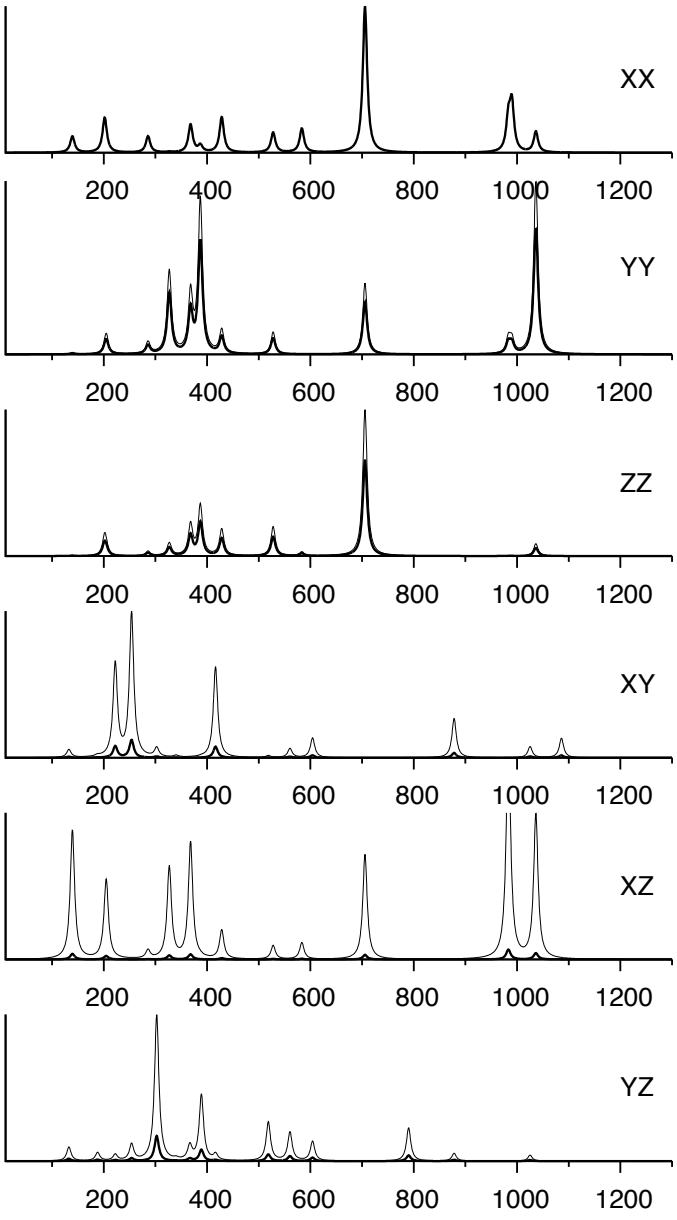

FIG. 5: Calculated single crystal directional Raman spectra of jadeite at 514 nm wavelength and 300 K. In all panels except the top one, the thin line reports the spectrum with a common normalization, while the thick line reports the intensity relative to the XX component.

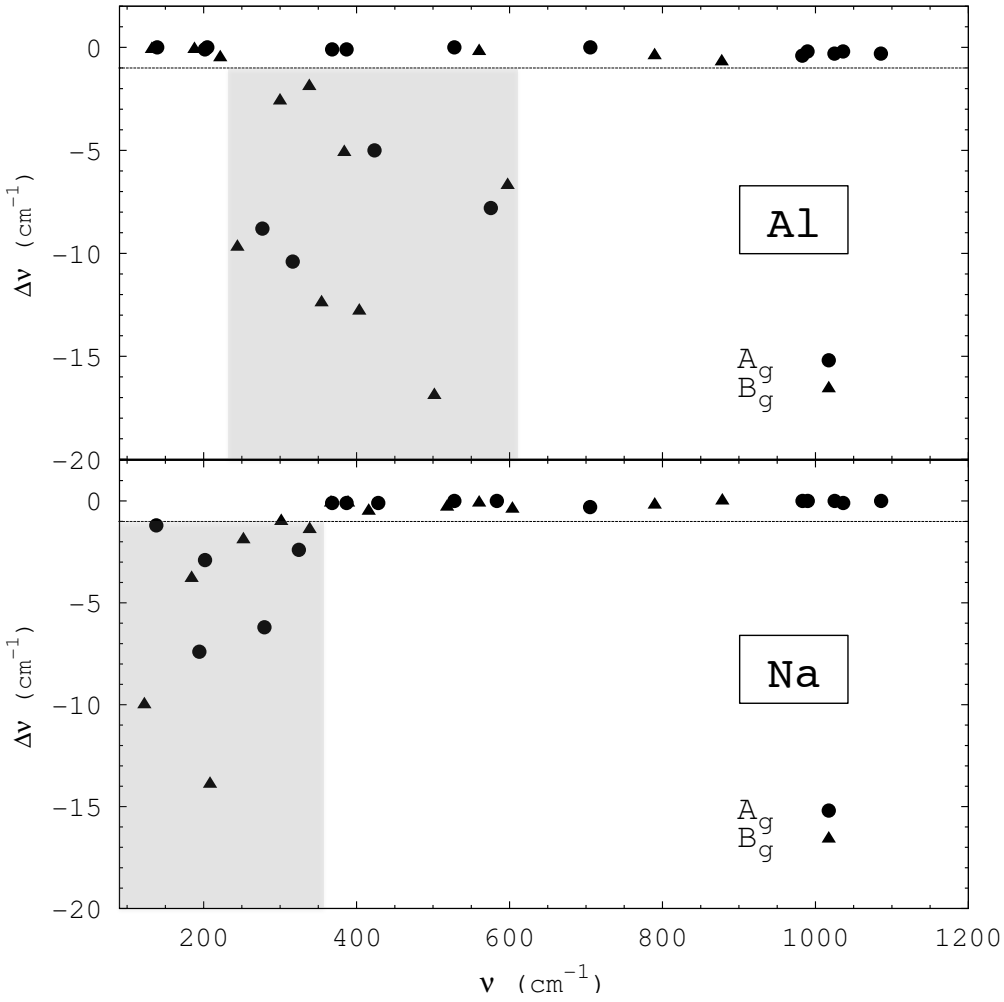

FIG. 6: "Isotopic" shift of the frequencies, $\Delta\nu$, of jadeite when the Al (upper panel) or Na (lower panel) mass is increased by 20%. The horizontal line at $\Delta\nu$ =-1 cm^{-1} separates large from small/negligible shifts.

Tables

	Calc.	Exp.	%Diff.
a (Å)	9.55	9.43	1.3
b (Å)	8.64	8.57	0.8
c (Å)	5.29	5.22	1.3
β (°)	108.04	107.58	0.4
V (Å^3)	414.87	402.15	3.2

TABLE I: Calculated and experimental[43] unit cell parameters of jadeite. Percentage differences are also reported.

		Calculated		Experimental					
				Gendron[12]			Downs[13]		
Mode	Symm.	ν	I	ν	$\Delta\nu$	I	ν	$\Delta\nu$	I
1	B_g	133	16.3	-	-	-	128	5	21
2	A_g	139	80.3	145	-6	m,w	145	-6	73
3	B_g	188	7.7	193	-5	h,w	-	-	-
4	A_g	202	156.5	203	-1	s,m	204	-2	370
5	A_g	205	60.6	-	-	-	-	-	-
6	B_g	222	60.9	221	1	w	223	-1	73
7	B_g	254	99.5	255	-1	m	256	-2	117
8	A_g	286	91.0	290	-4	w	295	-9	97
9	B_g	303	127.2	308	-5	m	310	-7	280
10	A_g	327	195.3	327	0	m	329	-2	222
11	B_g	340	2.3	-	-	-	-	-	-
12	B_g	367	12.0	-	-	-	-	-	-
13	A_g	368	315.5	373	-5	s	375	-7	836
14	A_g	387	439.7	383	4	h	-	-	-
15	B_g	389	55.0	-	-	-	-	-	-
16	B_g	416	59.2	-	-	-	-	-	-
17	A_g	428	236.3	430	-2	m,mc	434	-6	186
18	B_g	519	33.6	-	-	-	-	-	-
19	A_g	528	185.7	523	5	m	524	4	209
20	B_g	560	29.3	-	-	-	559	1	37
21	A_g	583	81.7	573	10	w	575	8	98
22	B_g	604	28.2	-	-	-	589	15	49
23	A_g	706	1000.0	698	8	s	700	6	1000
24	B_g	790	27.8	777	13	w	780	10	114
25	B_g	878	39.9	-	-	-	889	-11	32
26	A_g	983	150.0	-	-	-	-	-	-
27	A_g	990	169.0	988	2	m,mc	986	4	193
28	B_g	1025	11.6	-	-	-	-	-	-
29	A_g	1036	466.8	1036	0	s,m	1040	-4	569
30	B_g	1086	11.8	-	-	-	1080	6	45
N					17			20	
$\overline{\Delta\nu}$					1			0	
$\lvert\overline{\Delta\nu}\rvert$					4			6	
$\lvert\Delta\nu\rvert_{\max}$					13			15	

TABLE II: Calculated and experimental[12,13] Raman frequencies (ν, in cm^{-1}) and relative intensities of jadeite. $\Delta\nu$ is the difference $\nu_{\mathrm{calc}} - \nu_{\mathrm{exp}}$. In the statistics given at the bottom of the table, N is the number of peaks considered, $\overline{\Delta\nu}$ is the mean difference in frequency, $\overline{|\Delta\nu|}$ is the mean absolute difference, and $|\Delta\nu|_{\mathrm{max}}$ is the maximum absolute difference. In the Gendron spectrum, the intensities are classified as strong (s), medium (m), weak (w), composite (c) and shoulder (h). Square brackets group modes that represent unresolved bands in the Downs spectrum (see text). The sum of the calculated intensities of these modes shows good agreeement with the experimental intensity of unresolved bands.

[1] R. Dovesi, M. De La Pierre, A. M. Ferrari, F. Pascale, L. Maschio, and C. M. Zicovich-Wilson. The IR vibrational properties of six members of the garnet family: a quantum mechanical ab initio study. *Am. Mineral.*, 96:1787–1798, 2011.

[2] C. Carteret, M. De La Pierre, M. Dossot, F. Pascale, A. Erba, and R. Dovesi. The vibrational spectrum of $CaCO_3$ aragonite: combined experimental and a quantum mechanical investigation. *J. Chem. Phys.*, 138:014201–1–014201–12, 2013.

[3] M. De La Pierre, C. Carteret, R. Orlando, and R. Dovesi. Use of ab initio methods for the interpretation of the experimental IR reflectance spectra of crystalline compounds. *J. Comput. Chem.*, 34:1476–1485, 2013.

[4] R. Demichelis, H. Suto, Y. Noël, H. Sogawa, T. Naoi, C. Koike, H. Chihara, N. Shimobayashi, M. Ferrabone, and R. Dovesi. The infrared spectrum of ortho-enstatite from reflectance experiments and first-principle simulations. *Mon. Not. R. Astron. Soc.*, 420:147–154, 2012.

[5] L. Maschio, B. Kirtman, M. Rérat, R. Orlando, and R. Dovesi. Ab initio analytical RAMAN intensities for periodic systems through a coupled perturbed Hartree-Fock/Kohn-Sham method in an atomic basis set. I. Theory. *J. Chem. Phys.*, 139(16):164101, 2013.

[6] L. Maschio, B. Kirtman, M. Rérat, R. Orlando, and R. Dovesi. *Ab Initio* Analytical Raman Intensities for Periodic Systems through a Coupled Perturbed Hartree-Fock/Kohn-Sham Method in an Atomic Orbital Basis II: Validation and Comparison with Experiments. *J. Chem. Phys.*, 139(16):164102, 2013.

[7] L. Maschio, B. Kirtman, R. Orlando, and M. Rérat. *J. Chem. Phys.*, 137:204113, 2012.

[8] R. Dovesi, V. R. Saunders, C. Roetti, R. Orlando, C. M. Zicovich-Wilson, F. Pascale, B. Civalleri, K. Doll, N. M. Harrison, I. J. Bush, Ph. D'Arco, and M. Llunell. *CRYSTAL 2014 User's Manual*. University of Torino, Torino, 2013.

[9] L. Maschio, B. Kirtman, S. Salustro, C. M. Zicovich-Wilson, R. Orlando, and R. Dovesi. The raman spectrum of pyrope garnet. a quantum mechanical simulation of frequencies, intensities and isotope shifts. *J. Phys. Chem. A*, 2013.

[10] W. Deer, R. Howie, and J. Zussman. *An introduction to the rock forming minerals*. John Wiley, New York, 1992.

[11] D. C. Smith and F. Gendron. Archaeometric application of raman microprobe to the non-

destructive identification of two pre-columbian ceremonial polished 'greenstone' axe-heads from mesoamerica. *J. Raman Spectrosc.*, 28:731–738, 1997.

[12] F. Gendron, D. C. Smith, and A. Gendron-Badau. Discovery of jadeite-jade in guatemala confirmed by non-destructive raman microscopy. *J. Archeol. Sci.*, 43:837–851, 2002.

[13] R.T. Downs (2006) The RRUFF Project: an integrated study of the chemistry, crystallography, Raman and infrared spectroscopy of minerals. Program and Abstracts of the 19th General Meeting of the International Mineralogical Association in Kobe, Japan. O03-13.

[14] A. D. Becke. Density-Functional Thermochemistry 3. The Role of Exact Echange. *J. Chem. Phys.*, 98:5648–5652, 1993.

[15] W. Koch and M. C. Holthausen. *A Chemist's Guide to Density Functional Theory.* Wiley-VCH Verlag GmbH, Weinheim, 2000.

[16] C. M. Zicovich-Wilson, F. Pascale, C. Roetti, V. R. Saunders R. Orlando, and R. Dovesi. The calculation of the vibration frequencies of α-quartz: the effect of Hamiltonian and basis set. *J. Comput. Chem.*, 25:1873–1881, 2004.

[17] F. Pascale, M. Catti, A. Damin, R. Orlando, V. R. Saunders, and R. Dovesi. Vibration frequencies of $Ca_3Fe_2Si_3O_{12}$ andradite. An *ab initio* study with the CRYSTAL code. *J. Phys. Chem. B*, 109:18522–18527, 2005.

[18] F. Pascale, C. M. Zicovich-Wilson, R. Orlando, C. Roetti, P. Ugliengo, and R. Dovesi. Vibration frequencies of $Mg_3Al_2Si_3O_{12}$ pyrope. An *ab initio* study with the CRYSTAL code. *J. Phys. Chem. B*, 109:6146–6152, 2005.

[19] C. M. Zicovich-Wilson, J. Torres, F. Pascale, L. Valenzano, R. Orlando, and R. Dovesi. The *ab initio* simulation of the IR spectra of Pyrope, Grossular and Andradite. *J. Comput. Chem.*, 29:2268–2278, 2008.

[20] L. Valenzano, A. Meyer, R. Demichelis, B. Civalleri, and R. Dovesi. Quantum-mechanical ab-initio simulation of the Raman and IR spectra of $Mn_3Al_2Si_3O_{12}$ Spessartine. *Phys. Chem. Mineral*, 36:415–420, 2009.

[21] A. M. Ferrari, L. Valenzano, A. Meyer, R. Orlando, and R. Dovesi. Quantum-mechanical ab initio simulation of the raman and ir spectra of fe3al2si3o12 almandine. *Journal of Physical Chemistry A*, 113(42):11289–11294, 2009.

[22] L. Valenzano, F. Pascale, M. Ferrero, and R. Dovesi. Ab initio Quantum-Mechanical Prediction of the IR and Raman Spectra of $Ca_3Cr_2Si_3O_{12}$ Uvarovite Garnet. *Int. J. Quantum Chem.*,

110:416–421, 2010.

[23] R. Dovesi, L. Valenzano, F. Pascale, C.M. Zicovich-Wilson, and R. Orlando. Ab initio quantum-mechanical simulation of the Raman spectrum of grossular. *J. Raman Spectrosc.*, 40:416–418, 2009.

[24] L. Maschio, M. Ferrabone, A. Meyer, J. Garza, and R. Dovesi. The Infrared Spectrum of Spessartine $Mn_3Al_2Si_3O_{12}$ an *Ab Initio* All Electron Simulation with Five Different Functionals (LDA, PBE, PBESOL, B3LYP and PBE0) . *Chem. Phys. Lett.*, 501:612–618, 2011.

[25] M. De La Pierre, R. Orlando, L. Maschio, K. Doll, P. Ugliengo, and R. Dovesi. Performance of six functionals (LDA, PBE, PBESOL, B3LYP, PBE0 and WC1LYP) in the simulation of vibrational and dielectric properties of crystalline compounds. The case of forsterite Mg_2SiO_4. *J. Comput. Chem.*, 32:1775–1784, 2011.

[26] M. Prencipe. Simulation of vibrational spectra of crystals by ab initio calculations: an invaluable aid in the assignment and interpretation of the Raman signals. The case of jadeite ($NaAlSi_2O_6$). *J. Raman Spectrosc.*, 43:1567–1569, 2012.

[27] W. Koch and M. C. Holthausen. *A Chemist's Guide to Density Functional Theory.* Wiley-VCH Verlag GmbH, Weinheim, 2000.

[28] R. Dovesi, C. Roetti, C. Freyria Fava, M. Prencipe, and V.R. Saunders. On the elastic properties of lithium, sodium an potassium oxide. an ab initio study. *J. Chem. Phys.*, 156:11–19, 1991.

[29] M. Prencipe, I. Scanavino, F. Nestola, M. Merlini, B. Civalleri, M. Bruno, and R. Dovesi. High-pressure thermo-elastic properties of beryl ($Al_4Be_6Si_{12}O_{36}$) from ab initio calculations, and observations about the source of thermal expansion. *Phys. Chem. Mineral*, 38:223–239, 2011.

[30] R. Dovesi, C. Pisani, C. Roetti, and V. R. Saunders. *Phys. Rev. B*, 28:5781, 1983.

[31] M. Causà, R. Dovesi, C. Roetti, and V. R. Saunders. *J. Phys. Chem.*, 92:909, 1988.

[32] K. Doll, V. R. Saunders, and N. M. Harrison. Analytical hartree-fock gradients for periodic systems. *Int. J. Quantum Chem.*, 82:1–13, 2001.

[33] K. Doll. Implementation of analytical hartree-fock gradients for periodic systems. *Comput. Phys. Comm.*, 137:74–88, 2001.

[34] B. Civalleri, Ph. D'Arco, R. Orlando, V. R. Saunders, and R. Dovesi. *Chem. Phys. Lett.*, 348:131–138, 2001.

[35] C. G. Broyden. The Convergence of a Class of Double-rank Minimization Algorithms 1. General

Considerations. *J. I. Math. Appl.*, 6:76–90, 1970.

[36] R. Fletcher. A new approach to variable metric algorithms. *Comput. J.*, 13:317–322, 1970.

[37] D. Goldfarb. A Family of Variable-Metric Methods Derived by Variational Means. *Math. Comput.*, 24:23–26, 1970.

[38] D. F. Shanno. Conditioning of quasi-Newton methods for function minimization. *Math. Comput.*, 24:647–656, 1970.

[39] M. Veithen, X. Gonze, and Ph. Ghosez. Nonlinear optical susceptibilities, Raman efficiencies, and elctro-optic tensors from first-principles density functional perturbation theory. *Phys. Rev. B*, 71:125107, 2005.

[40] L. Maschio, B. Kirtman, M. Rérat, R. Orlando, and R. Dovesi. Comment on "*Ab Initio* analytical infrared intensities for periodic systems through a coupled perturbed hartree-fock/kohn-sham method" [j. chem. phys. 132, 204113 (2012)].

[41] M. Ferrero, M. Rérat, B. Kirtman, and R. Dovesi. Calculation of first and second static hyperpolarizabilities of one- to three-dimensional periodic compounds. Implementation in the CRYSTAL code. *J. Chem. Phys.*, 129:244110, 2008.

[42] M. Ferrero, M. Rérat, R. Orlando, and R. Dovesi. The calculation of static polarizabilities of periodic compounds. The implementation in the CRYSTAL code for 1D, 2D and 3D systems. *J. Comput. Chem.*, 29:1450–1459, 2008.

[43] `http://www.mindat.org/min-2062.html`.